Electronic Supplementary Material (ESI) for Journal of Materials Chemistry B.

Supporting Information

Materials. N-Isopropylacrylamide (NIPAM), N,N'-Methylenebisacrylamide (BIS), silver nitrate ($AgNO_3$), sodium borohydride ($NaBH_4$), ascorbic acid, sodium hydroxide, poly(ethylene glycol) (PEG, MW 6000), 2-hydroxy-2-methylpropiophenone (photo-initiator) were purchased from Sigma-Aldrich (USA) and used as received.

Synthesis of macroporous PNIPAM Hydrogels. 0.1785 g NIPAM monomer, 0.0575 g PEG (MW 6000) and 0.0226 g BIS were dissolved in 1 mL Nanopure water in a glass vial. A 2.25 μL of photoinitiator (2-hydroxy-2-methylpropiophenone) was then added. The vial was shaken by hand to make a homogeneous solution mixture. Two pieces of glass slides were separated by parafilms with a thickness of 0.5 mm, which was used as a holder for the monomer solution. The monomer solution and the holder were kept in a refrigerator (4 ℃) for 30 minutes. Then the monomer solution was injected to the holder. The polymerization was conducted by using a hand-hold UV lamp with 254 nm as the excitation wavelength. During the polymerization, the holder was kept on a glass petri dish which floated on the surface of an ice-water bath. After the polymerization, the hydrogel was immersed in a large amount of water for at least 1 day to leak out the unreacted chemicals, non-cross-linked polymers and PEG. Then the hydrogel was cut into a rectangular shape (length: 1.70 cm; width: 0.85 cm) or other shapes (star, stripe, disk, etc) for the fabrication of PNIPAM-AgNPs hybrid hydrogels.

Synthesis of PNIPAM-AgNPs Hybrid Hydrogels. The silver nanoparticles (AgNPs) were grown *in situ* within the macroporous PNIPAM hydrogel sheet. Briefly, the macroporous PNIPAM hydrogel sheet was immersed in 2 mL $AgNO_3$ solution (0.04 mg/mL) for 30 minutes. It was then transferred to a plastic petri dish and 5 mL freshly-prepared $NaBH_4$ (0.4 mg/mL) was added to reduce the silver nitrate within the hydrogel for 30 minutes to obtain silver (Ag) seeds. The Ag-seed-containing hydrogel sheet was put in water to remove excess $NaBH_4$ on its surface and then immersed in 2 mL $AgNO_3$ growth solution (1.7 mg/mL) in a glass vial for 30 minutes. A 200 µL of ascorbic acid (17.6 mg/mL) was then added to the growth solution, followed by the quick addition of 200 µL sodium hydroxide (40 mg/mL) while gently shaking the vial. After 5 minutes, the vial was put in a 29 ºC water bath for 2 hours. Finally the hybrid hydrogel sheet was put in 29 ºC water which slowly cooled down to room temperature. Before doing light-mediated shape transformation, the hybrid hydrogel sheet was immersed in a large amount of water for at least 24 h for the AgNPs to stabilize in the hydrogel. We point out that the hybrid hydrogel sheet can be kept in water for two years without losing the ability in shape transformation when subject to NIR light. For the control experiments, we fabricated macroporous hydrogel but without loading AgNPs. We also synthesized non-porous hydrogel without using PEG, the pore-forming reagent. Then we loaded AgNPs in the non-porous hydrogel *in situ* by using the same experimental conditions as that for macroporous hybrid sheet. These hydrogels were also subject to NIR light irradiation. We found that the the pristine macroporous hydrogel sheet without AgNPs barely deformed (Fig. S22). We also found that the non-porous hybrid sheet would slowly and slighly deformed under NIR irradiation (Fig. S23).

Light-Triggered Shape Transformations. An 808 nm laser (MDL-N-808, Changchun New Industries Optoelectronics Technology Co., Ltd, China) was used as the light source and it worked at 5 watts throughout the experiments. During the experiments, the hybrid hydrogel was immersed in 100 mL water in a glass petri dish. Aluminum foil was used to make the photo mask which was attached onto a glass slide. The distance between the laser and the glass slide was adjusted to make sure the light spot took on the shape indicated by the photo mask.

Hydrogel Swelling. The swelling property of the hybrid hydrogel sheet was characterized by using the swelling ratio which was measured gravimetrically after wiping off the excess water on the hydrogel's surface with a piece of Kim wipes in the temperature range from 22 to 36

°C. The hybrid hydrogel sheet was incubated in a water bath for at least 48 h at each temperature. The swelling ratio was calculated by using the following formula[1]

$$\text{Swelling ratio} = W_s/W_d$$

where W_s is the weight of the swollen hydrogel at the particular temperature and W_d is the dry weight of the hydrogel.

Mechanical Property. An AR2000 stress-controlled rheometer (TA Instruments) was used to study the mechanical properties of the hybrid hydrogel sheet. Rheological experiments were performed at 22 °C and 32 °C, respectively by using cone-and-plate geometry (25 mm diameter and 2^o cone angle). A solvent trap was used to minimize drying of the sample during measurements. Dynamic stress-sweep experiments were first performed on the sample to identify its linear viscoelastic (LVE) region at different temperatures and dynamic frequency sweeps were then performed within the LVE region.

FTIR Measurements. The compositions of the hydrogel sheet were analyzed by FTIR in the region of 650-4000 cm^{-1}. Before the measurement, the hydrogel samples were swollen for at least two days at room temperature and then were freeze-dried for 24 h. The dried hydrogel samples were directly put under the FTIR probe and the spectra were taken, which was shown in Fig. S1. From Fig. S1, it can be seen that the compositions of pure PNIPAM hydrogel, macroporous PNIPAM hydrogel and macroporous PNIPAM-AgNP hybrid hydrogel were the same. There exists a typical -C=O stretch band of PNIPAM at around 1644 cm^{-1} and a representative -N-H vibration band of PNIPAM at about 1538 cm^{-1}. In addition, there is no typical -C-O stretch band of PEG at around 1100 cm^{-1}. These findings indicated that the PEG only acted as a pore-forming agent and did not react with the NIPAM monomer in the fabrication of PNIPAM hydrogel. The same conclusion was also reached in the previous report on macroporous PNIPAM hydrogel synthesized via a redox method[1].

Optical Property of Hybrid Hydrogel Sheet. The optical property of the hybrid hydrogel sheet was characterized by measuring its absorbance using UV-Vis spectroscopy (Lambda 40 UV/VIS Spectrometer, PerkinElmer, USA). Briefly, swollen hybrid hydrogel sheet and macroporous PNIPAM hydrogel sheet of the same size were put onto a glass slide respectively. The excess water on the glass slide was removed by using Kim wipes to make sure the hydrogel sheet attached to the glass slide. Then the glass slides were put in the reference and sample light paths respectively. The hydrogel sheets were adjusted to be of the same position on the glass slides. The UV/VIS spectra were then taken in an absorption mode at a slit width of 1 nm, scanning speed of 480 nm/min and data interval of 1 nm. The spectrum was shown in Fig. S2, from which it can be seen that the hybrid hydrogel sheet had a high absorbance (around 1.0) at 808 nm. Since a pristine macroporous gel without Ag nanoparticles was used as the reference, the UV-vis spectrum of the hybrid hydrogel reflects the plasmonic absorption of Ag nanoparticles rather than the scattering of the gel.

Surface Morphology of Hydrogel Sheet. The surface morphologies (Fig. S3) of the macroporous PNIPAM hydrogel and hybrid hydrogel sheet were studied by using scanning electron microscopy (XL Series-30, Philips, USA). Samples of the freeze-dried hydrogels were coated with carbon (JFC-1200 Fine Coater, Japan) prior to the SEM examination. From Fig. S3 a), it can be seen that the macroporous PNIPAM hydrogel sheet had a macroporous structure with pore sizes estimated to be in the range of 200 nm to 1 μm. After AgNPs were fabricated within the hydrogel, the pore size remained similar as that in the macroporous PNIPAM hydrogel (see Fig. S3 b)). As Fig. S3 c) showed, there was a sharp difference between the surface of the hybrid hydrogel sheet and its cross-section. As seen from Fig. S4, the hybrid hydrogel has a very dark and shiny appearance indicating silver nanoparticles were aggregated on the surface (left image in Fig. S4). We claim that the photothermal property of the hybrid hydrogel sheet under the 808 nm light was mainly due to the absorbance of the AgNPs from the hydrogel surface.

Photothermal Property of Hybrid Hydrogel Sheet. The photothermal property of the hybrid hydrogel sheet was studied by photothermal imaging technique. The set-up of this experiment was shown in Fig. S5. Briefly, the hybrid hydrogel sheet was immersed in 100 mL water in a glass petri dish and was irradiated with an 808 nm laser at a power of 5W for 2 min and then the laser was shut off for another 3 min. During the irradiation, the laser spot that reached the hydrogel sheet took on a stripe shape due to the photomask used. The surface temperature of the hybrid hydrogel sheet was monitored by using a FLIR SC300 infrared camera (FLIR, Arlington, VA). Real-time thermal images were captured with frame rate at 60 Hz, and analyzed by FLIR Examiner software. The result was shown in Fig. S6. It can be clearly seen that a remarkable thermal gradient (ranging from 22 ºC to 32 ºC) was created on the sheet's surface when the sheet was locally irradiated with NIR light (Fig. S6a). During the irradiation, the thermal gradient on the sheet's surface gradually propagated with the increase of the irradiation time. A stable thermal gradient ranging from 22 ºC to 32 ºC was eventually established on the sheet's surface. We found that the hybrid hydrogel sheet started to bend while its surface temperature increased from 21 °C to 32 °C during the irradiation process and it went back to its original shape when it cooled down. We point out here that that the surface temperature of the hybrid hydrogel sheet can increase to 40 °C by reducing the distance between the laser and the hydrogel surface (data not shown).

Finite Element Modeling on Shape Transformations of a Hybrid Hydrogel Sheet.

Free energy model of temperature-responsive hydrogel. In our PNIPAM hydrogel, the interacting aggregation of cross-linked polymer chain network and solvent molecules constitutes a thermodynamic system of which the macroscopic behaviors are governed by its thermodynamic energetics. The deformation of PNIPAM hydrogel in balance with mechanical loads and a solvent reservoir can be modeled by the framework developed by Cai and Suo[2]. By thermodynamics consideration, the Helmholtz free energy of a swelling hydrogel arises from two origins: i) the stretching of the polymer network and ii) the mixing of the two species of molecules. Hence the free energy density function takes the form:

$$W = \frac{1}{2}NkT[F{:}F - 3 - 2log(J)] + kT\left[clog\left(\frac{vc}{1+vc}\right) + \frac{(A_0 + B_0T)c}{1+vc} + \frac{(A_1 + B_1T)c}{(1+vc)^2}\right] \tag{1}$$

where W is the free energy per unit volume in the dry state, N is the number of polymer chains per unit volume in the dry state, k is Boltzmann constant, T is the current temperature at the material point, **F** is the deformation gradient tensor which takes the original dry state as reference frame, J is the Jacobian of deformation gradient tensor, i.e., J=det(**F**), v is the molecular volume of water, c is the relative concentration of solvent molecules in the hydrogel-solvent aggregation, and A_0, B_0, A_1 and B_1 are parameters related to the enthalpy of mixing. The first term in Equation (1) denotes that the stretching of polymer chain network obeys a neo-Hookean hyperelastic material law, and the second term implies that the mixing of PNIPAM polymer and water molecules follows the Flory-Huggins theory of solution[3]. A_0, B_0, A_1 and B_1 in Equation (1) are to be fitted to the experimental data for different temperature-responsive hydrogels, as we will identify in the immediate section for our PNIPAM-AgNPs hybrid hydrogel.

Equation (1) specifies the explicit expression of the free energy density function which takes the extensive variables **F**, c as well as the intensive variable T as its arguments. In such cases that the hydrogel is put in contact with a stable aqueous reservoir, the chemical potential of solvent molecule μ is constant; then upon Legendre transformation, the free energy density W is carried to its corresponding thermodynamic potential:

$$\hat{W}(F, \mu, T|N, A_0, B_0, A_1, B_1) = W(F, c, T|N, A_0, B_0, A_1, B_1) - \mu c \tag{2}$$

thus $\hat{W}$ is a natural function of **F**, μ and T.

When the stress level is adequately low so that no new void or pore is generated in the hydrogel, the volumetric change of the material solely results from the migration of solvent molecules; hence the deformation **F** and solvent concentration c are correlated by^4:

$$J = 1 + vc \tag{3}$$

Substitute Equations (1) and (3) into Equation (2), one arrives at the explicit form of $\hat{W}$:

$$\begin{aligned}\hat{W}(F, \mu, T | N, A_0, B_0, A_1, B_1) \\ = \frac{1}{2} NkT[F{:}F - 3 - 2log(J)] + \frac{kT}{v}(J-1)\left[log\left(\frac{J-1}{J}\right) + \frac{(A_0 + B_0 T)}{J} + \frac{(A_1 + B_1 T)}{J^2}\right] - \frac{\mu}{v}\end{aligned} \tag{4}$$

Free swelling of PNIPAM hydrogel in water and determination of parameters. When submerged in an aqueous environment with homogeneous temperature field, a piece of free standing PNIPAM hydrogel, in the absence of pre-introduced stress, will swell (or contract) freely in response to the uniformly varying temperature field. The free swelling case satisfies the condition that the hydrogel deforms uniformly in any three orthogonal directions and that the hydrogel retains its stress-free state since neither deformation mismatch nor mechanical constraint exists. For such a homogeneous deformation the principal stretch ratios have identical value, and the deformation gradient tensor becomes

$$F = \begin{bmatrix} \lambda & 0 & 0 \\ 0 & \lambda & 0 \\ 0 & 0 & \lambda \end{bmatrix} \tag{5}$$

where λ is the uniform stretch ratio. And in this case the volumetric ratio $J = V/V_0 = \lambda^3$, where V is the volume of the hydrogel piece in the deformed state and V_0 is the volume in the reference (dry) state.

As discussed above the stress tensor vanishes:

$$S_{ik}(F, \mu, T | N, A_0, B_0, A_1, B_1) = \frac{\partial \hat{W}}{\partial F_{ik}} = 0 \tag{6}$$

Equation (6) yields the relation between stretch ratio λ and temperature T in the free swelling case. In addition, if the chemical potential of water is known and set to zero, then T can be readily expressed by the following equation:

$$T = -\frac{Nv(\lambda^5 - \lambda^3) + \lambda^6 \log(1 - \lambda^{-3}) + \lambda^3 + (A_0 + A_1\lambda^{-3})}{B_0 + \lambda^{-3}B_1} \tag{7}$$

The equation above dictates the temperature required by the principle of minimum free energy, in free swelling cases, for the temperature-sensitive hydrogel to maintain certain amount of deformation. In other words it also depicts how the hydrogel deforms in response to the change of the homogeneous temperature field.

By fitting the function $T(\lambda|\mathbf{S}=0, \mu=0)$ to the experimentally obtained $T \sim J$ relation, we determined the parameters Nv, A_0, B_0, A_1 and B_1. Fig. S7 shows the fitted curve of volumetric ratio $V/V_0 = \lambda^3$ as a function of temperature T, with the specified parameters: Nv=0.03317, A_0=-2.5418, B_0=0.01081, A_1=0.57099, B_1=-0.000418. We will use this set of parameters for our PNIPAM hydrogel in the following calculations.

Model of heat transfer processes. When the top surface is exposed to NIR laser, the AgNPs embedded in PNIPAM absorb the photons and convert the light energy into heat, the surrounding hydrogel matrix is thus heated. In order to benchmark the thermal properties of our PNIPAM hydrogel, we setup the transient heat transfer model for a hydrogel piece with length L_d=1.7cm, width w_d=0.85cm and thickness t_d=0.5mm (same dimensions as the hydrogel piece in the NIR light irradiation experiment). The initial temperature of the entire body is the same as ambience temperature T_0=295K. Then the top surface of the hydrogel piece is brought to exposure to two adjacent laser stripes with width w_l=0.2cm and heat flux intensity H=1.2 J·cm^{-2}·s^{-1}, and the bottom surface away from the laser irradiation is set to the constant ambience temperature. Laser is switched on for 120 seconds and is shut down thereafter to let the hydrogel cool down through heat dissipation into the environment.

Keeping track of the temporal evolution of the highest temperature on the top surface, we are allowed to compare the temperature response curve with the experimental data and determined the thermal diffusivity of PNIPAM hydrogel $\alpha=K/\rho C_p=2.36\times10^{-5}$ cm^2/s, where K, ρ and C_p denote the thermal conductivity, density, and specific heat of the material respectively. The temperature contour of the top surface and the highest temperature evolution are shown in Fig. S6b with comparison to the thermography.

Deformation of PNIPAM hydrogel in inhomogeneous temperature field. The deformation behavior of a temperature-sensitive hydrogel is governed by a thermodynamic free energy thus resembling a hyperelastic material[2,4]. Each thermodynamic equilibrium state of temperature-sensitive hydrogel is a local minimum of the system free energy which can be fully defined by the stretch ratios λ and a dependent solvent molecule concentration c as discussed above. Furthermore, the thermodynamic equilibrium is to be altered upon the change of environment variables. Therefore besides of being able to respond to the conventional mechanical loads, such materials as PNIPAM hydrogels are also able to deform in accordance with the change in temperature and chemical potential.

Solving for the equilibrium states is a boundary value problem (BVP). For simpler cases, e.g., free swelling hydrogel with homogeneous temperature, analytical solution can be obtained, whereas for more complicated case, e.g., hydrogel swelling in an inhomogeneous temperature field, the BVP can be solved numerically by FEM. We adopted the FEM framework established by Ding *et al.* for the temperature-responsive hydrogel[5], and prescribed the material properties determined above to the PNIPAM hydrogel used in this study. At this stage we assume that the deformation of PNIPAM hydrogel will not affect the heat transfer processes. A fully coupled thermo-mechanical algorithm is implemented in the commercial FEM package ABAQUS by making use of its temperature-displacement elements.

We investigated the impact of the heat flux intensity H and the laser stripe width w_l on the deformation of the PNIPAM hydrogel piece. A 2-D plane strain model of 1.7cm×0.5mm hydrogel is exposed to a stripe-shaped laser irradiation with heat flux intensity H and width w_l. The heat transfer process from the top surface towards the bottom side creates temperature gradient within the hydrogel body. Dictated by the minimization of free energy the hotter part of the PNIPAM hydrogel tends to shrink more than the cooler part, whereas the deformation of one material particle has to be constrained by its neighbors to achieve thermodynamic equilibrium. Therefore this deformation mismatch causes the hydrogel piece to bend towards the side of elevated temperature.

We plotted the dimensionless curvature (κt_d) at the geometric center as the indicator of localized deformation and the dimensionless transverse deflection (h/t_d) as the measurement of overall deformation (see Fig. 6c, Fig. 6d and Fig. S8). Higher heat flux intensity leads to a higher temperature on the top surface thus results in an increased temperature gradient in the thickness direction of the hydrogel piece, which in turn promotes the localized deformation at the deformation tip. If the light stripe is wider, the temperature at heat transfer equilibrium will also be higher. Moreover the wider laser stripe makes a larger portion of hydrogel to contribute to the total deformation and as a result the deflection is larger. As Fig. 6c, Fig. 6d and Fig. S8 indicate, the curvature at the tip and the deflection in lateral direction both increases as H and w_l increase.

Additionally, if a PNIPAM hydrogel piece is brought to exposure to a fixed power laser source, i.e., the total quantity of energy absorbed by the hydrogel is fixed at certain amount ($P=Hw_l=const$), there exists an optimal combination of H and w_l which yields the largest deflection. As shown in Fig. S9(a), the wider laser stripe comes with a lower intensity and a narrower one comes with a higher intensity if the laser source power is fixed at $P=Hw_l=3.6$ J/s. Fig. S9(a) also shows the temperature field in the reference state and the stress field in the deformed state. The stress scale is normalized by $kT_0/v\lambda_0^3$, where the Boltzmann constant k=1.3806×10^{-23} m^{2}kg·s^{-2}K^{-1}, the initial temperature T_0=295K, the initial stretch ratio λ_0=1.5489 (at T_0=295K and relative to the dry state), and the molecular volume of water v=2.9922×10^{-29} m^3. Upon the increasing w_l the intensity H decreases and the resulting localized deformation is deduced (Fig. S9(b)). However the deflection of the hydrogel piece has a maximum at w_l=0.2cm, this is because the deflection indicates the level of the total deformation of the entire piece. The increasing w_l brings a larger part of hydrogel into irradiation, while the amount of heat which per unit area of top surface receives is reduced. The tradeoff between the increasing number of contributors and decreasing amount of the contribution per share allows the existence of the maximum deflection.

Heat transfer model with convection boundary condition

Effects of finite convection

The light responsive deformation behavior of the hybrid hydrogel depends on the heat transfer process inside the hydrogel which establishes an asymmetric temperature field triggering the directional bending towards the laser source side . The heat transfer process is determined by two main factors, namely the energy flux input from the laser and the heat dissipation through convection into the ambience . In the model presented in the Main Text, we fixed the temperature on the back surface of the hydrogel at the ambience temperature. This case corresponds to the maximum convection condition on the back surface, i.e., the convection coefficient is infinite so that the energy dissipates at the highest rate. As a result, the back surface temperature of the hybrid hydrogel sheet equals the temperature of its surrounding water . Such a treatment is valid only if approach such as forced convection is implemented.

To investigate the effect of finite convection on the evolution of temperature and deformation, we prescribed finite convection boundary condition on the hydrogel surface, in addition to the heat flux over the central section of the top surface. Because the water molecules inside the hydrogel network still retained mobility of migrating back and forth between the network and the ambience, the convection coefficient was set at a moderate value 700 $Wm^{-2}K^{-1}$, and the ambience temperature was set at the room temperature 295K.

We used the angle change α to quantify the bending deformation. Fig. S10 showed the temporal evolution of α for different heat flux inputs. When heat flux was comparatively small (e.g., H=3 and 3.5W/cm^2), α increased monotonically with time and converged to an equilibrium state value of 29.5° at ~6s. In all the other cases where H>3.5W/cm^2, the angle reached a maximum value and started to decay. For example, when H=3.5W/cm^2, α reached a peak value 35.2° at 1s, then gradually reduced to a steady state value at 21.6^o. Compared to the fixed temperature boundary condition, the heat dissipation was smaller for the finite convection case, thus temperature field was established at a higher rate, which resulted in a fast deformation response: at the maximum bending angle, the highest temperature in the center of the top surface was 315K, and the back surface was heated up to 301K. A temperature difference of 14K was developed in ~1s. In addition, with finite convection both the top and back surfaces were heated to a higher temperature. The elevated temperature on the back surface leaded to a reduction of the bending angle. As shown in Fig. S11, the globule/coil phase transition of PNIPAM was accomplished at ~305K, and the volumetric deformation in the top layers reached its saturation. Therefore, any further temperature increase only resulted in the shrinkage in the back layers, pulling the hydrogel piece away from its initial deformation, which in turn reduced the bending angle. As indicated by the temperature profiles at the equilibrium state in Fig. S10, even though the temperature difference between the top/back surfaces at the maximum deformation state (14K) was slightly smaller than that at the final state (15K), the bending angle was 13.6° larger. This was because the increase of the top surface temperature from 315K to 327K was not accompanied with any further shrinkage, whereas the volume of the back-layer reduced as the temperature increased from 301K to 312 K. This resulted in the reduction of bending angle from the maximum bending state.

To compare the deformation capability of the hydrogel piece under finite and infinite convection boundary conditions, the bending angle was plotted in Fig. S12 against the top/back surface temperature difference. At first, the hydrogel with finite convection deformed more. This was because 1) the top surface temperature was higher with finite convection , and 2) the heat-affected zone was larger near the top. When $\Delta T>15$K, these two factors were overcome by increased temperature in the back-layer and the deformation was larger for the infinite convection case. The dashed line showed the bending angle in the equilibrium state.

Impact of the ambience temperature

In all the aforementioned calculations, we set the ambience temperature at 295K. Upon further illumination, the local temperature of water near the hydrogel piece will also increase due to its weak absorption of NIR light. To understand the effect of the increased ambience temperature, we set the ambience temperature at 300K over the 3.5mm section in the center of the back surface, and left the ambience temperature around all the other surfaces at 295K. The applied 5W/cm^2 heat flux remained the same as the baseline case. The bending angle declined to 12.7° from 23.2° (Fig. S15). This further reduction of deformation corresponded to the dome collapse which was observed in the experiment for the thinner sheet (Fig. S16c). We pointed out our hybrid sheet system was very dynamic under light irradiation and its deformation was a result of a fine interplay between the heat transfer in the hydrogel and the dissipation into the environment.

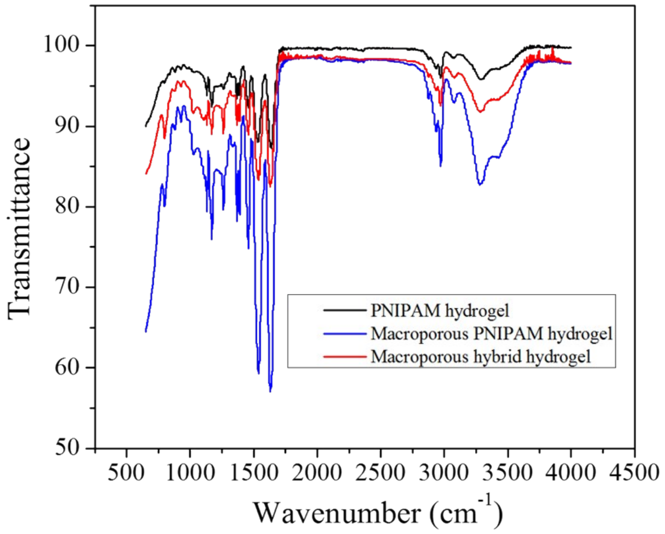

Fig. S1 FTIR measurement of PNIPAM hydrogel, macroporous PNIPAM hydrogel and macroporous hybrid PNIPAM-AgNP hydrogel sheet. It indicated the PEG acted as a pore-forming agent in the PNIPAM hydrogel fabrication.

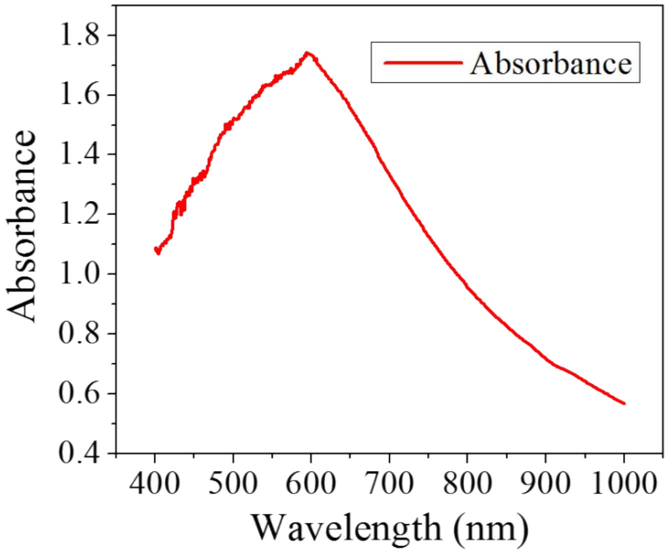

Fig. S2 UV-Vis absorption of the hybrid hydrogel sheet. The hybrid sheet had a sufficient absorption at 808 nm wavelength-that matches the wavelength of continuous-wave NIR laser-in order to produce sufficient thermal energy to trigger the shape transformations. Since a pristine macroporous gel without Ag nanoparticles was used as the reference, the UV-vis spectrum of the hybrid hydrogel reflects the plasmonic absorption of Ag nanoparticles rather than the scattering of the gel.

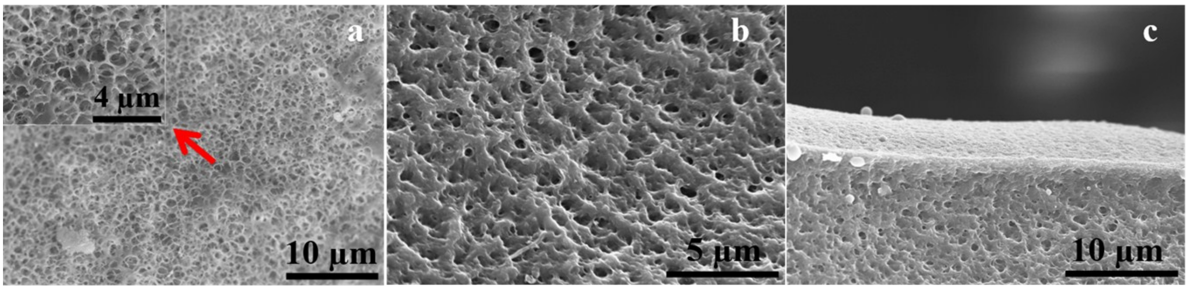

Fig. S3 SEM images of the surface morphology of macroporous PNIPAM hydrogel sheet and hybrid hydrogel sheet. a) surface morphology of macroporous PNIPAM hydrogel sheet; b) morphology of the cross-section of the hybrid hydrogel sheet; c) overall morphology of the cross-section of the hybrid hydrogel sheet. Inset: enlarged image of the region denoted by the red arrow.

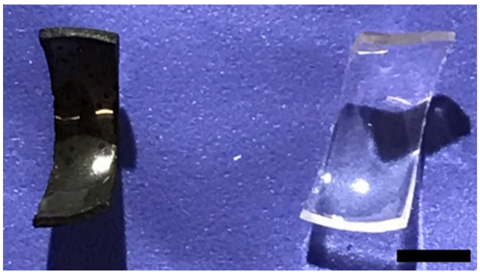

Fig. S4 Optical images of macroporous pristine PNIPAM hydrogel sheet (right image) and hybrid hydrogel sheet (left image). It can be seen that the gel surface of the hybrid sheet is dark and shining (rather than transparent as the pristine hydrogel sheet without Ag nanoparticles), indicating the presence of a high-density AgNPs on the sheet's surface. Scale bar: 0.2cm.

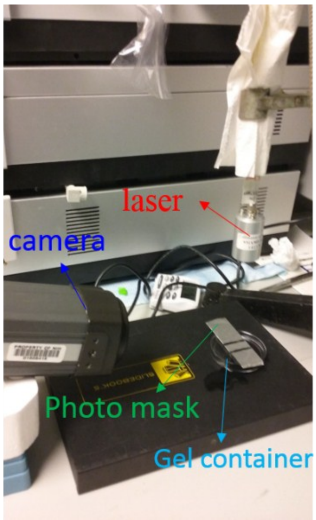

Fig. S5 Setup of photo-thermal imaging experiment. The camera was seeing the top-surface of the hybrid sheet.

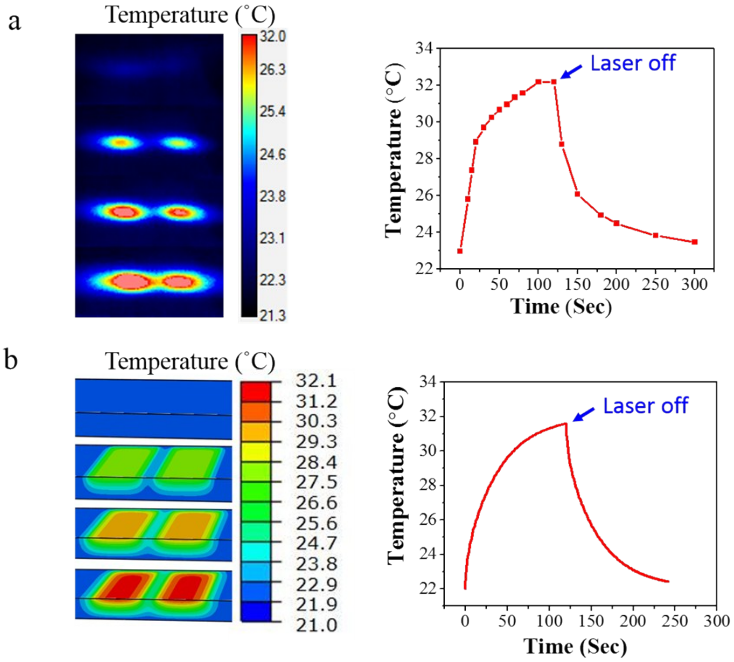

Fig. S6 Experimental study (a) and finite element analysis (b) of the generation of thermal gradient within hydrogel sheet upon NIR laser irradiation. The hybrid sheet was irradiated for 120 seconds and then the laser was switched off. The temperature was measured for an interval of 30 seconds. As can be seen from a), a stable thermal gradient ranging from 21 to 32 °C was established on the sheet's top surface under light irradiation, which was confirmed by FEM analysis. We used infinite convection boundary condition in the heat transfer model to calculate the temperature profile in the sheet under light irradiation.

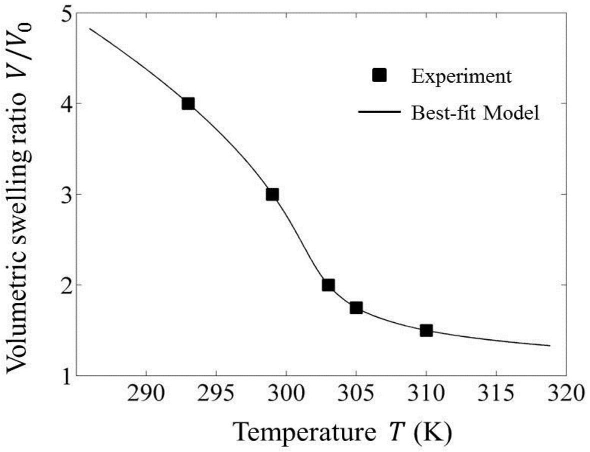

Fig. S7 Volumetric swelling ratio of macroporous PNIPAM hydrogel as a function of temperature. This curve is used to determine the parameters used in finite element modeling as described in the text of the supporting information

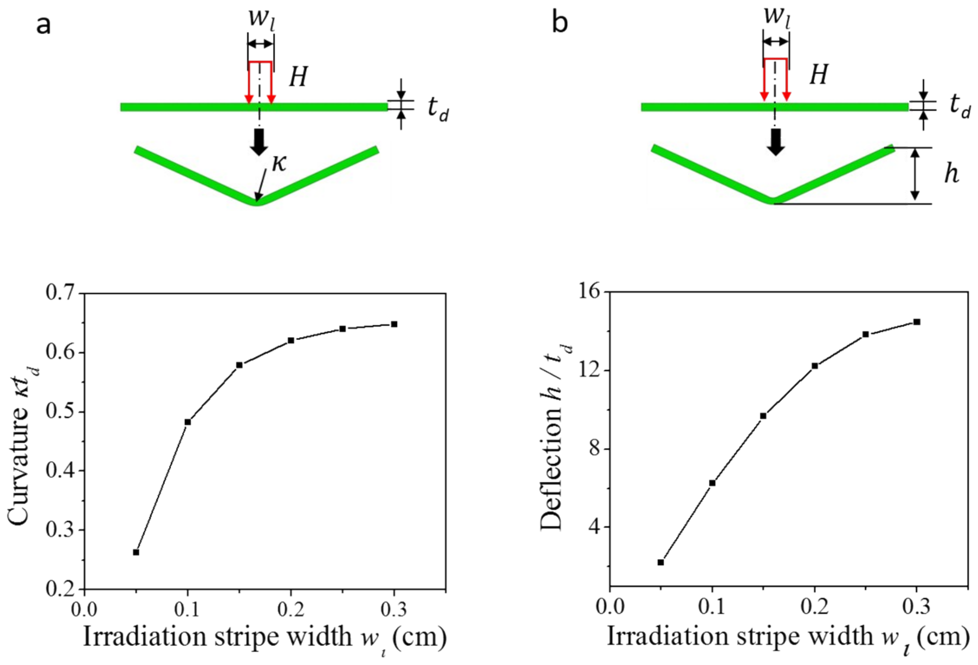

Fig. S8 Finite element modeling of effects of supplied light energy and irradiation stripe width on bending of the hybrid sheet. The bending increased with the increase of irradiation stripe width. a) Normalized curvature κt_d ; b) deflection h/t_d as a function of laser stripe width w_l at heat flux intensity H=1.8 J·cm^{-2}·s^{-1}

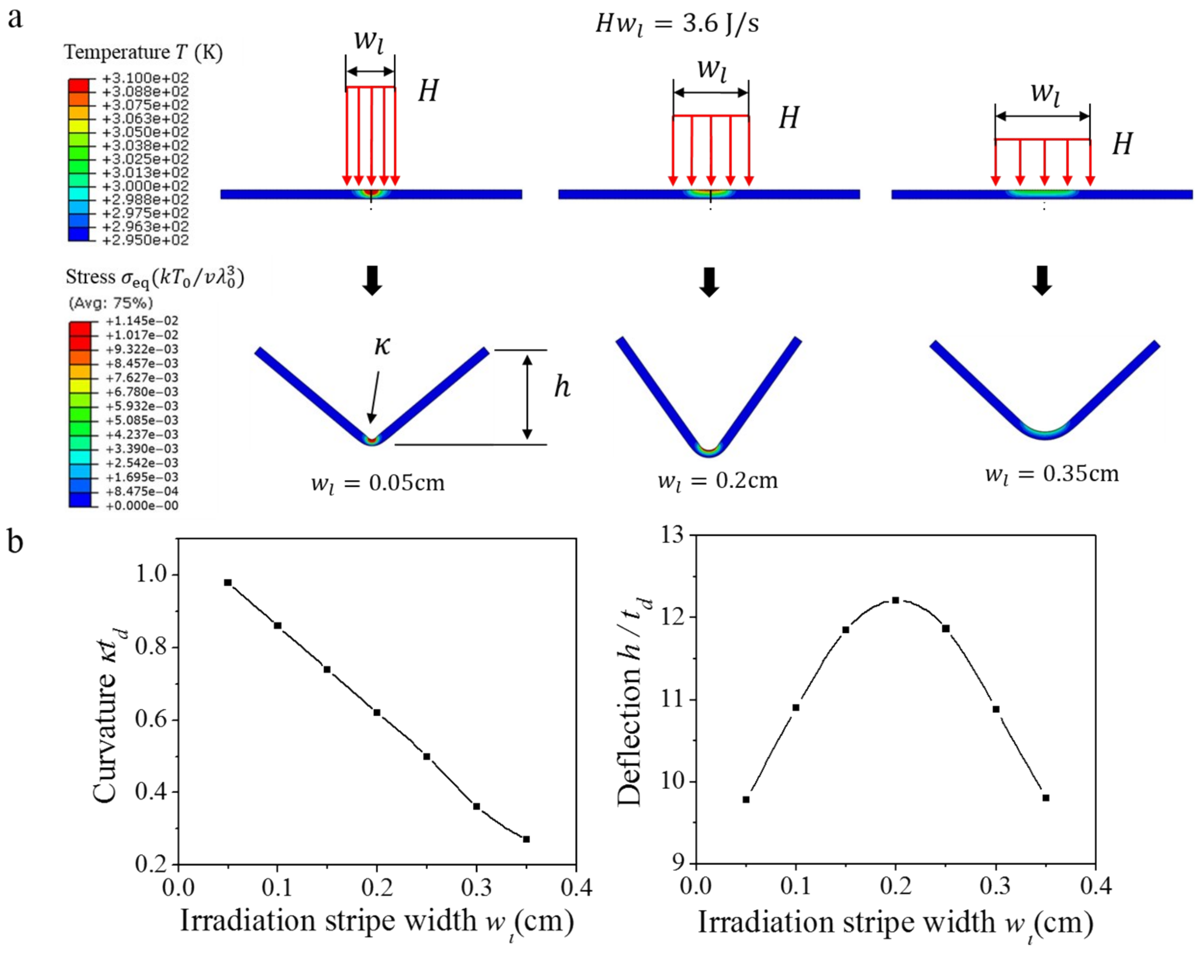

Fig. S9 Finite element modeling of the bending of the hybrid hydrogel sheet with respect to laser stripe width at a fixed total input energy. a) The hybrid hydrogel sheet was subject to laser stripes with the light input energy fixed at 3.6 J/s. b) Normalized curvature κt_d and deflection h/t_d as a function of laser stripe width w_l at fixed light input energy of 3.6 J/s. t_d is the thickness of the hybrid sheet which is 0.5 mm. The FEM analyses indicated that at a fixed light input energy, the bending curvature decreased with the increase of laser stripe width, while the overall deflection (h/t_d) reached a maximum when increasing the laser stripe width.

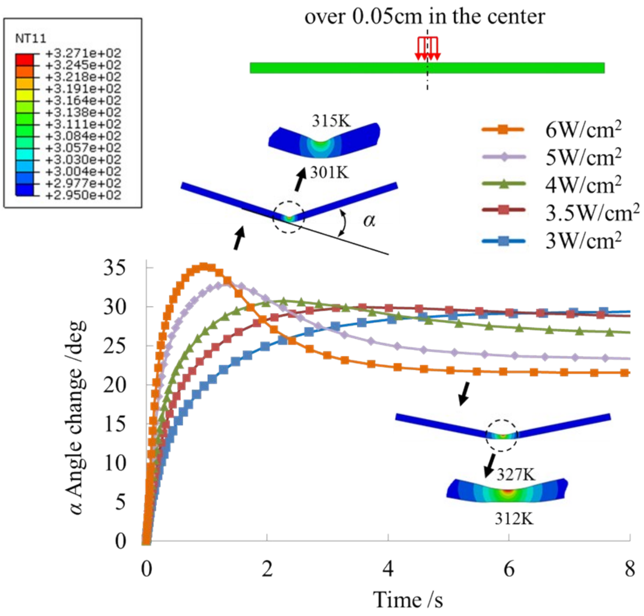

Fig. S10 Temporal evolution of the bending angle at various heat fluxes (H) into the center of the hydrogel. The color legend in top left side of the figure showed the temperature distribution at both the peak bending angle state, and at the steady state, when H=6W/cm^2.

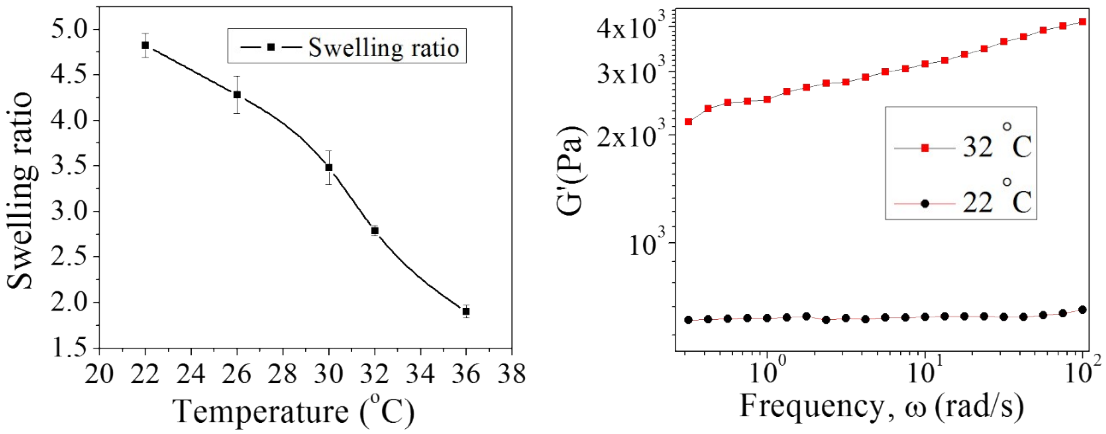

Fig. S11 Swelling and shear modulus of hybrid hydrogel sheet at different temperatures. The hybrid sheet had a gradual decrease in swelling when increasing the temperature. It became stiffer with the increase of temperature.

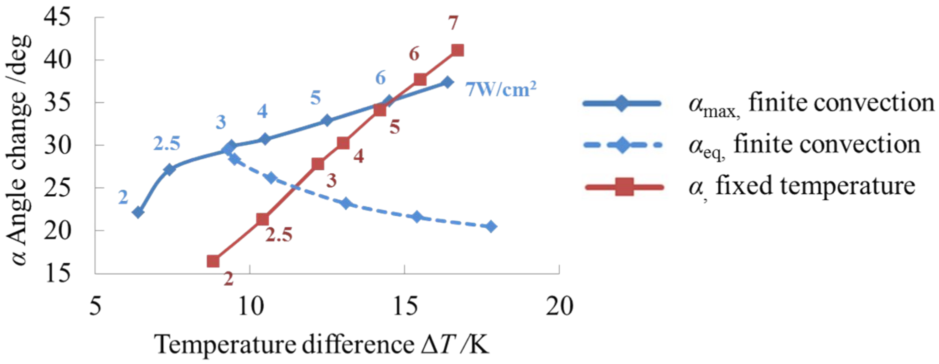

Fig. S12 Effect of temperature difference between sheet's top and bottom surface on its bending. The solid blue line showed the maximum bending angle under 700 $Wm^{-2}K^{-1}$ surface convection (finite convection condition), and the dashed line represented α in the steady state under same surface convection condition. The red line showed the bending angle for fixed temperature boundary condition. The number near the lines indicated the heat flux inputs.

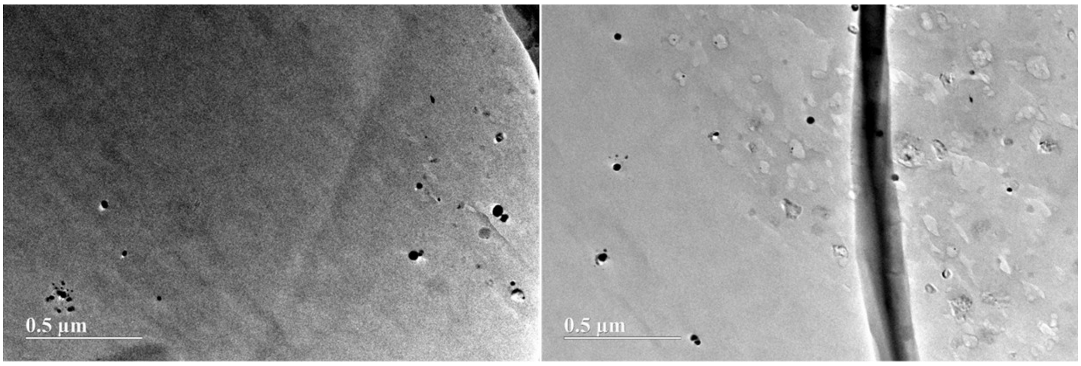

Fig. S13 TEM images of AgNPs within the hybrid hydrogel sheet. The AgNPs have a broad size distribution with roughly spherical shapes.

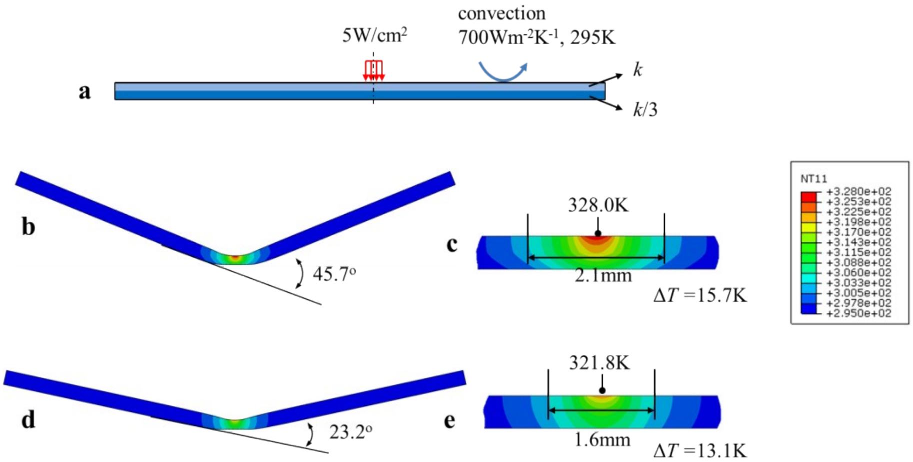

Fig. S14 a) Schematic of a double-layered hydrogel piece with different thermal conductivities k. b) Bending angle in steady state for double-layered hydrogel and d) for the baseline case. c) and e) The temperature profiles in the reference (undeformed) frame for both cases.

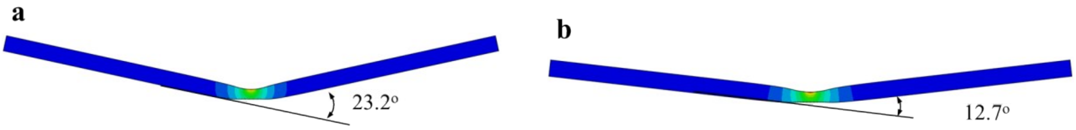

Fig. S15 Bending angle reduced from (a) 23.2° in the baseline case to (b) 12.7° if the ambience temperature increased to 300K over the center 3.5 mm section of the back surface.

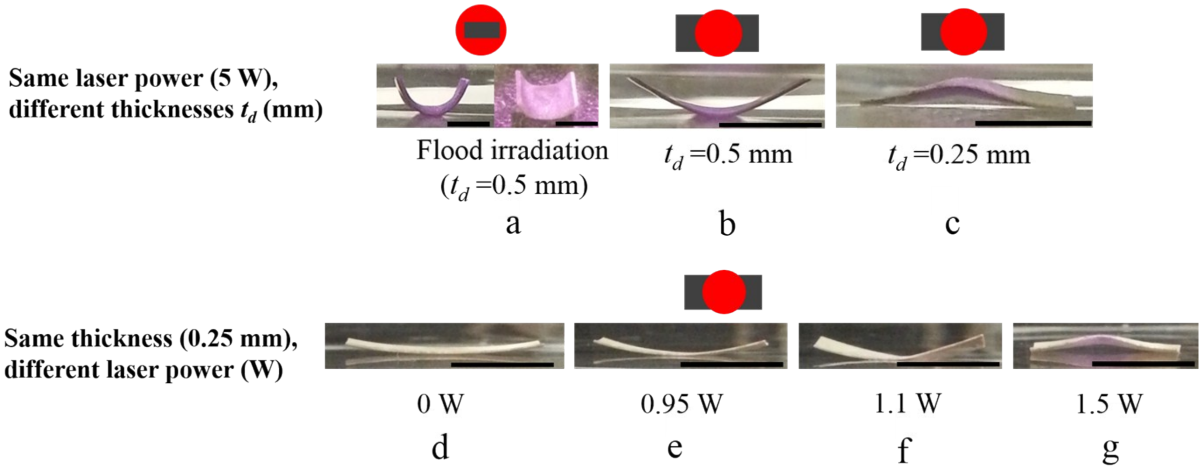

Fig. S16 Shape transformation of the hybrid hydrogel sheet under flood irradiation and the bending stability of the hybrid hydrogel sheet with respect to its thickness and the laser power. a) the sheet (length:1cm; width: 0.5cm) bent when its whole surface was subject to NIR irradiation indicating the thermal gradient along the sheet's surface might not play important roles in its shape transformation. b, c) the sheet (length: 1.8 cm; width: 0.9cm) suffered from a bending instability when its thickness reduced from 0.5 mm to 0.25 mm. c) the sheet bent but buckled downwards very quickly to form a saddle-like structure. d,e,f,g) indicated that a thinner sheet would have a stable bending at a low laser power. These findings suggested that the thickness-direction thermal gradient was necessary for the hybrid sheet to have a stable shape transformation. The scale bar in a) represents 0.5cm while those in b-g) represents 0.85cm.

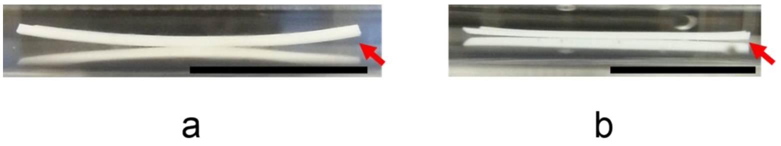

Fig. S17 Thickness-dependent natural curvature of macroporous PNIPAM hydrogel sheet (length: 1.7 cm; width: 0.9 cm). a) thickness: 0.5 mm; b) thickness: 0.125 mm. The hydrogel sheet bent less with the decrease of its thickness. The scale bar in the image represents 0.85 cm.

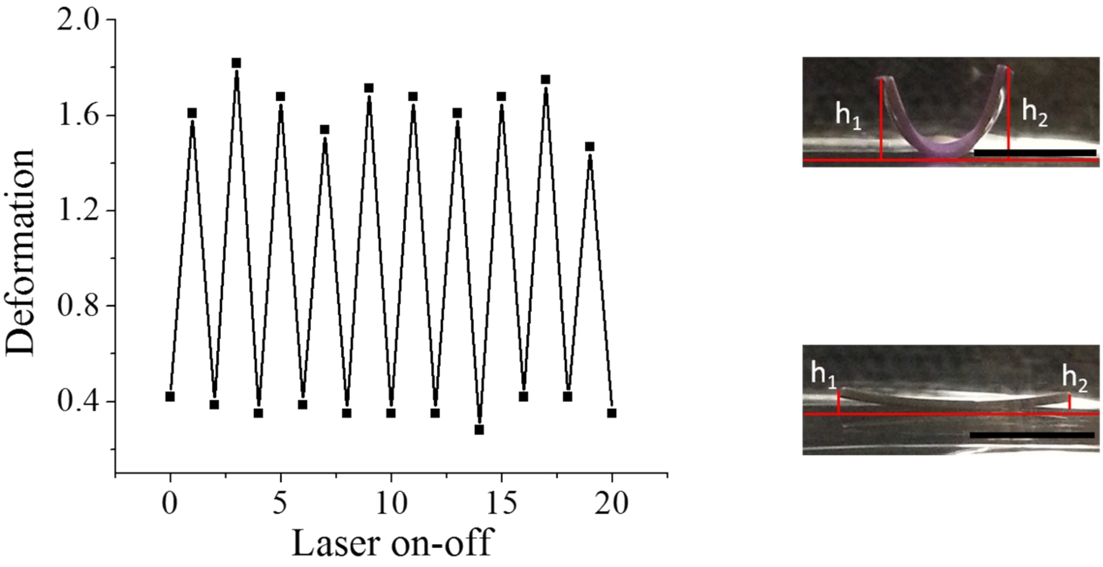

Fig. S18 Reversibility of shape transformations of hybrid hydrogel sheet in response to light. The deformation of the hoof-like structure was monitored in each laser on-off cycle. In each cycle, the hydrogel sheet reached its maximum deformation within 5 seconds and recovered its original shape within 5 minutes. The deformation was calculated as $(h_1+h_2)/(2t_d)$, where t_d is the thickness of the hybrid sheet which was 0.5 mm. The scale bar represents 0.85cm.

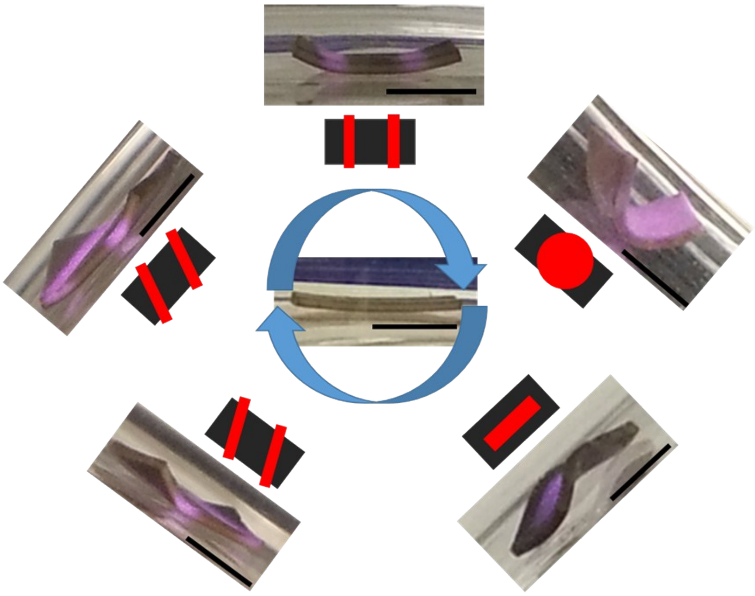

Fig. S19 Shape transformations of hybrid hydrogel sheet of reduced overall size (length: 1 cm; width: 0.5 cm; thickness: 0.5 mm). The shape transformations were smaller when reducing the overall size of the hybrid sheet. The scale bar represents 0.5cm.

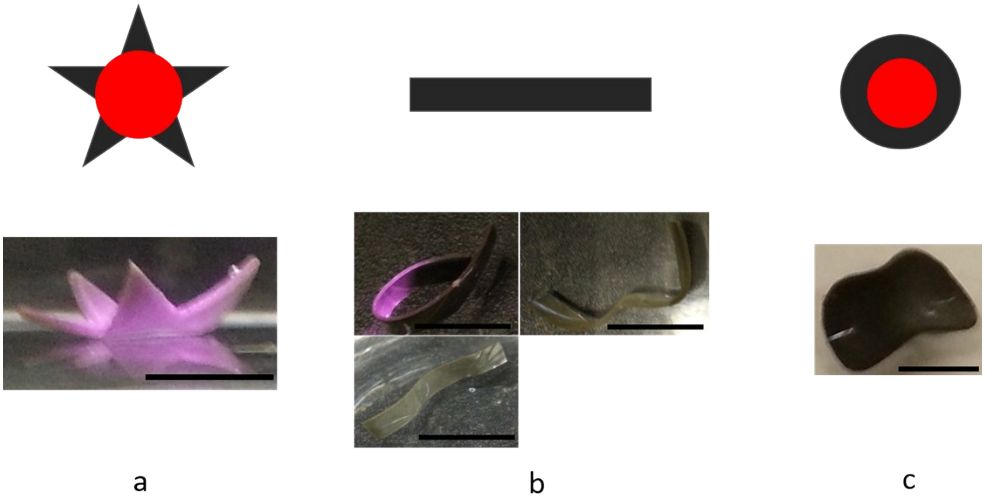

Fig. S20 Transformations from hybrid hydrogel sheets with different original shapes. Shapes in a ,c) were directly obtained via irradiation with a circular laser spot when the sheet was under water. Shapes in b) were achieved in water by quickly changing the irradiated area using a circular laser spot. The scale bar in a) and c) represents 0.85cm, while that in b) represents 2cm.

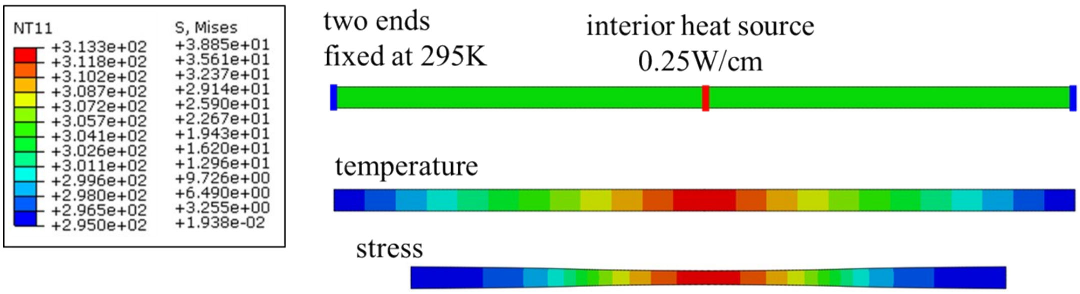

Fig. S21 Effect of z-direction thermal gradient on bending deformation of the hybrid sheet. In absence of z-direction thermal gradient, the hybrid sheet transformed to a kayak paddle shape with necking contraction in the middle instead of a bending deformation. Without the z-direction temperature gradient, the deformed hydrogel morphology retains the z-symmetry and does not bend. The z-direction thermal gradient, or the z-component of thermal gradient, breaks the z-symmetry in the thickness direction and results in a bending deformation.

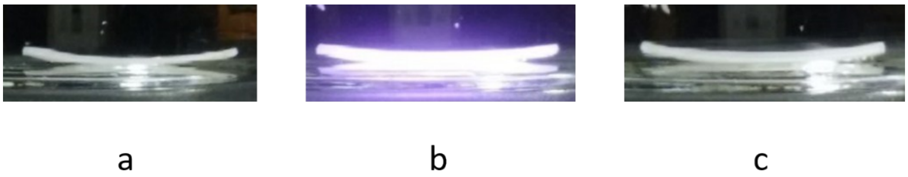

Fig. S22 Scattering of hydrogel network on the deformation. The macroporous hydrogel sheet without AgNPs was irradiated for 1 minute at a laser power density of 0.7 W/cm2. a) was the hydrogel before irradiation, b) was the hydrogel that has been irradiated for 1 minute, c) was the hydrogel right after switching off the laser after 1 minute irradiation. It can be seen that the contribution of the scattering of the hydrogel network to the deformation was negligible.

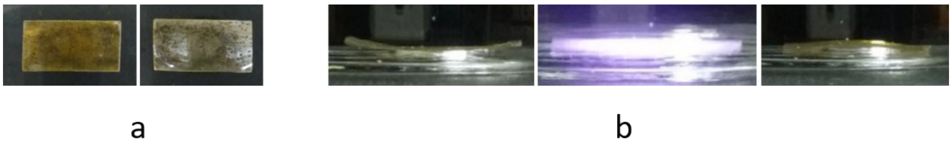

Fig. S23 Mechanical deformation of non-porous hybrid hydrogel sheet under NIR light irradiation. a) showed the top (left) and bottom (right) surfaces of the non-porous hybrid sheet; b) was the deformation of the non-porous hybrid sheet after NIR irradiation (808nm wavelength) for 3 minutes at a laser power density of 0.7 W/cm2. Left image in b) was the sheet before irradiation, middle image was the sheet under irradiation for 3 minutes while right image was the non-porous sheet right after switching off the laser.

References

1 X. Z. Zhang, Y. Y. Yang, T. S. Chung and K. X. Ma, *Langmuir* **2001**, *17*, 6094-6099.

2 S. Cai and Z. Suo, *J. Mech. Phys. Solids* **2011**, *59*, 2259-2278.

3 M. L. Huggins, *J.Chem.Phys.* **1941**, *9*, 440.

4 W. Hong, Z. Liu and Z. Suo, *Int. J. Solids Struct.* **2009**, *46*, 3282-3289.

5 Z. Ding, Z. Liu, J. Hu, S. Swaddiwudhipong and Z. Yang, *Int. J. Solids Struct.* **2013**, *50*, 2610-2619.